Wear 310 (2014) 51–62

Contents lists available at ScienceDirect

Wear

journal homepage: www.elsevier.com/locate/wear

Effects of sigma phase and carbide on the wear behavior of CoCrMo alloys in Hanks′ solution

Yan Chen [a], Yunping Li [b,*], Shingo Kurosu [b], Kenta Yamanaka [a], Ning Tang [b], Yuichiro Koizumi [b], Akihiko Chiba [b,**]

[a] Tohoku University, Department of Material Science and Engineering, Sendai 980-8579, Japan
[b] Institute for Material Research, Sendai 980-8577, Japan

ARTICLE INFO

Article history:
Received 9 September 2013
Received in revised form
6 December 2013
Accepted 11 December 2013
Available online 19 December 2013

Keywords:
CoCrMo alloy
σ phase
Carbide
Wear behavior
Contact mechanics
Surface fatigue

ABSTRACT

This study aims to elucidate the synergy effects of the σ phase and carbide on the wear behavior of low-carbon (LC) and high-carbon (HC) cobalt–chromium–molybdenum (CoCrMo) alloys, by using pin-on-disc tests under Hanks′ lubricated conditions. Fractured or torn-off σ-phase precipitates were observed to be the main reason for abrasion for both LC and HC alloys. Carbides were torn off at the initial high contact pressure to form pitting; σ-phase precipitates around the pitting were uprooted and led to micro cracks, which is considered as surface fatigue of HC alloy. In contrast, strain-induced martensite observed on the worn surface was contributed to the increase of hardness and abrasion resistance of LC alloy.

1. Introduction

Cobalt–chromium–molybdenum (CoCrMo) alloys have been widely used in gas turbines, dental and orthopedic implants [1–5], as the group of cobalt-base alloys can be commonly described as wear, corrosion and heat resistant [6]. Up to now, the largest use of wear resistant components and/or their applications appeal for persistent and further studies of CoCrMo alloy.

Properties of CoCrMo alloys can be improved by change of cobalt crystallographic nature, solid-solution-strengthening effect of alloying elements (Cr, Mo, W et al.), and formation of second phase such as carbides [7]. However, the alloys′ compositions of today are little changed from the early ones of Elwood Haynes but for tremendous amount and type of carbide formation in the microstructure [6]. Therefore, plenty of researches focusing on how carbides affect the wear behavior of the CoCrMo alloy have been conducted. Fulcher et al. [8] and Desai et al. [9] found that the abrasive wear resistance increased monotonically with increasing volume fraction and size of the carbide phase, respectively, for a series of CoCr alloys. Cawley et al. [10] also reported that the as-cast CoCrMo alloy containing the highest volume fraction of blocky carbide showed the lowest wear rate. Similar conclusions were drawn by Scholes and Unsworth [11] and Tipper et al. [12], who suggested that the improved hardness and wear resistance could be attributed to the presence of carbides in wrought CoCrMo alloys. However, the opposite viewpoint that the hard precipitate phases (e.g., $M_{23}C_6$-type carbides) are detrimental to the wear behavior was also espoused by Wimmer et al. [13] and Chiba et al. [14], because hard carbide is prone to being torn off from the rubbing surfaces, resulting in three-body abrasive wear. It could be concluded that the type, distribution, morphology and volume fraction of carbide have significant influence to wear resistance for various CoCrMo alloys.

In the typical carbon- and nitrogen-containing CoCrMo alloy system, the precipitation of carbide and σ phases is unavoidable since most hot working and heat treatments are carried out below ~1373 K [15,16]. However, no detailed observation on interaction between the carbide and σ phases on the wear behaviors of these alloys has been identified so far. Therefore, the aim of the present study is to elucidate the synergy effects of the σ phase and carbide on the wear behavior of CoCrMo alloys by performing pin-on-disc wear tests in Hanks′ lubricated environment.

2. Experimental procedure

2.1. Materials

The materials used in this study are low-carbon (LC) and high-carbon (HC) Co–28Cr–6Mo alloys, with the compositions listed in

* Corresponding author. Tel.: +81 22 215 2452; fax: +81 22 215 2116.
** Corresponding author. Tel.: +81 22 215 2115; fax: +81 22 215 2116.
E-mail addresses: chenyan@imr.tohoku.ac.jp (Y. Chen), lyping@imr.tohoku.ac.jp, yunpinglee@gmail.com (Y. Li), kurosu@imr.tohoku.ac.jp (S. Kurosu), k_yamanaka@imr.tohoku.ac.jp (K. Yamanaka), ningtang@imr.tohoku.ac.jp (N. Tang), koizumi@imr.tohoku.ac.jp (Y. Koizumi), a.chiba@imr.tohoku.ac.jp (A. Chiba).

0043-1648/$ - see front matter
http://dx.doi.org/10.1016/j.wear.2013.12.010

Table 1
Chemical compositions of LC and HC alloys (wt%).

Ingots	Co	Cr	Mo	C	Si	Mn	N
LC	Bal.	27.7	5.5	0.05	0.52	0.55	0.13
HC	Bal.	27.6	5.5	0.27	0.65	0.57	0.14

Table 1. Hot forging process for the ingots were: (1) vacuum induction melting process; (2) heating to 1523 K at a heating rate of 1 K/s with a homogenization holding for 18 h, followed by air cooling; (3) hot forging at 1273 K with a total reduction of ~45%; and (4) water quenching. The mechanical properties were evaluated in hardness tests (Shimadzu, HMV) and Young′s modulus measurements, and the densities were evaluated using the Archimedes method.

2.2. Microstructure characterization

Pins and discs were machined to dimensions of ϕ 6 mm × 20 mm and ϕ 30 mm × 5 mm, respectively. The spherical contact ends of the pins (*SR* 2.4 mm) were ground with emery paper of up to #6000 grit and polished with a silica suspension. The discs were prepared with a sequence of polishing with 180–1200 grit emery papers, 30-min polishing with alumina and silica suspensions, and finally electropolishing in an electrolyte (methanol:sulfuric acid = 9:1) at 6 V, room temperature. The microstructure of disc surface was observed by performing scanning electron microscopy (SEM, Hitachi S3400N), electron probe microanalysis (EPMA, JXA-8530F, JEOL) and transmission electron microscope (TEM, JEM-2000EX II). The phase constitution of the matrix was identified by performing X-ray diffraction (XRD, Philips X′ Pert) measurements with Cu $K\alpha$ radiation over $40^\circ < 2\theta < 55^\circ$, focused on three locations on each disc. Elaborate XRD measurements were performed using the monochrome model over $35^\circ < 2\theta < 55^\circ$ to determine the second phase precipitates.

2.3. Pin-on-disc test

All the specimens were ultrasonically cleaned with distilled water and ethanol (Kaijo sonocleaner 200D), then dried for 21.6 ks at room temperature in an air atmosphere in advance. The pin-on-disc test was conducted using a RHSCA FRP-2000 tribometer, as shown schematically in Fig. 1. The pin was mounted with a 9.8 N load representing a harsh contact (initial contact pressure: 1.69 GPa) [17], and tested against a disc rotating at 20 mm/s (24 rpm). The temperature was set to 37 ± 2 °C in an argon atmosphere, and the rotation radius was 8 mm. The lubricant was Hanks′ solution, with its composition listed in Table 2. The test was performed over a continuous period of 60.48 ks for a total sliding distance of ~12.1 km. All tests were repeated 3 times for both LC and HC alloys.

The worn specimens were cleaned ultrasonically in distilled water and ethanol, and then dried for weight loss measurement using a direct-reading balance (Shimadzu AUW 320). The wear factor was calculated according to the most frequently used equation [18]

$$\omega_s = M_{loss}/(w \times s \times \rho) \tag{1}$$

where M_{loss} is weight loss, w is the normal load, s is the sliding distance, and ρ is the density of the specimen. The worn surfaces were analyzed using XRD, SEM and laser microscope (LM, Keyence KV-x200 series). The phase volume fractions were quantitatively

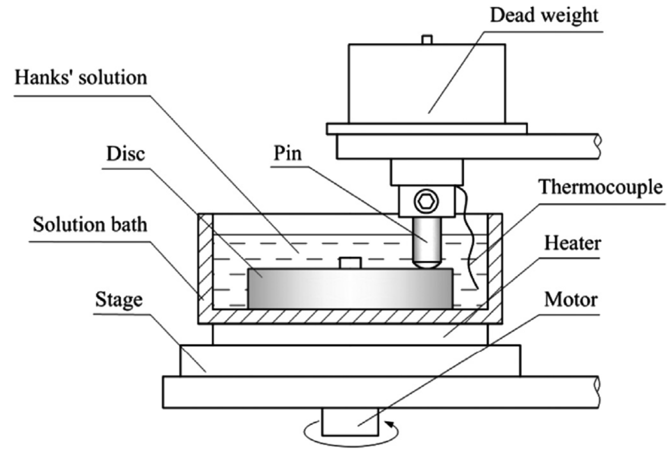

Fig. 1. Schematic diagram showing the basic working principle of the pin-on-disc test.

Table 2
Chemical composition of Hanks′ solution (g/L).

NaCl	KCl	$CaCl_2$	$NaHCO_3$	$Na_2HPO_4 \cdot 2H_2O$	KH_2PO_4	$MgSO_4 \cdot 7H_2O$
8.0	0.4	0.14	0.35	0.06	0.06	0.2

Table 3
Basic properties of LC and HC alloys.

	LC	HC
Density (g/cm^3)	8.4	8.3
Young′s modulus (GPa)	220	220
Vickers hardness, HV1	420	447

calculated according to Eq. (2), as proposed by Sage and Guillaud [19]

$$\frac{x}{1-x} = \frac{1}{4} \times \frac{1.85}{0.27} \times \frac{I_{(2\ 0\ 0)\gamma}}{I_{(1\ 0\ \bar{1}\ 1)\varepsilon}} \tag{2}$$

where x is the volume fraction of the face cubic centered γ phase and $I_{(2\ 0\ 0)\gamma}$ and $I_{(1\ 0\ \bar{1}\ 1)\varepsilon}$ are the integrated intensities of the (2 0 0)γ and $(1\ 0\ \bar{1}\ 1)\varepsilon$ peaks, respectively.

The cross section of the worn surface was cut by a focused ion beam (FIB, QUANTA 200 3D, FEI) and observed using TEM. The hardness and roughness of as-polished and worn surfaces were evaluated with a Vickers hardness tester (Shimazu, HMV), a stylus profilometer (Surfcorder DSF 500) and LM, respectively. The wear debris was isolated from the Hanks′ solution by Omnipore membrane filter paper (Millipore 0.2 μm JG, Ireland), then dispersed ultrasonically in ethanol for 30 min for SEM observation.

3. Results

3.1. Material characterization

The properties of the alloys are tabulated in Table 3. Both LC and HC alloys have densities of ~8.3 g/cm^3 and Young′s moduli of ~220 GPa. The initial Vickers hardness, HV1, of the HC alloy is a little higher that of LC alloy as the strength hardening effect of carbide.

Fig. 2 shows the microstructure with equiaxed grains of ave. ~20 μm for (a) LC and (b) HC alloys, in which globular precipitates were observed predominantly precipitating along the grain

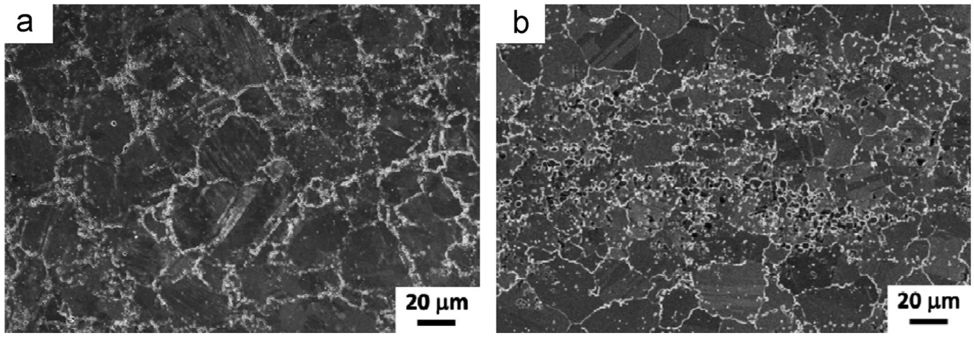

Fig. 2. SEM micrographs showing the original microstructure of (a) LC and (b) HC alloys, in which precipitates can be observed inside the grains or along the grain boundaries.

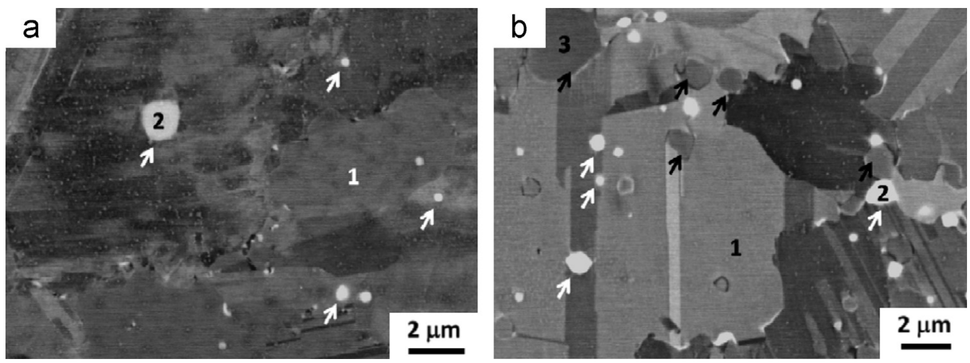

Fig. 3. Compositional images showing the bright and dark precipitated phases indicated by white and black arrows, respectively, for (a) LC and (b) HC alloys, in which some points were numbered for EPMA analyses.

boundaries, or some of them inside the grains. Attention should be paid that some precipitates tend to segregate along the rolling direction during hot forging, as a result of temperature difference between the center and the surface of HC ingot.

The details of the precipitated phases in the matrix are shown in the compositional images (Fig. 3). Fig. 3(a) shows bright precipitates in the LC alloy, as indicated by white arrows, whereas Fig. 3(b) shows both the bright and larger dark ones in the HC alloy, with the latter feature indicated by black arrows. It is noted that more bright precipitates were observed in the HC alloy, and they tended to form around the dark precipitate/matrix interface. The volume fractions of the bright phase were roughly estimated to be 1.1% and 3.7% for LC and HC alloys, respectively, by means of image processing. EPMA analysis results of the precipitates and matrix at the numbered positions are listed in Table 4. It was observed that the bright precipitates at positions 2 are rich in Mo and Si, whereas the larger dark precipitate at position 3 is rich in Cr, Mo, and C as compared to the matrix at positions 1. Combined with the elaborate X-ray profiles of the precipitates shown in Fig. 4 and the phase diagram for the Co–28Cr–6Mo system [15], the bright and dark precipitates were verified to be the σ phase and $M_{23}C_6$ (M=Cr, Mo) carbides, respectively. TEM results (Fig. 5) showed a typical eutectic $M_{23}C_6$ carbide precipitated in the HC matrix. It should also be noted that the Cr_2N phase was not observed in the SEM micrographs of the present alloys, probably because it is homogeneously dissolved throughout the matrix as nanosized particles [16,20].

The phase constitutions of the disc surfaces before and after the wear test were analyzed by XRD spectra, as shown in Fig. 6(a) and (b), respectively. Before the wear test, both LC and HC alloys showed a dominant γ-phase matrix. However, after the wear test, slight increases in the ε phase peak intensity were observed on the worn surfaces, indicating that the strain-induced martensitic transformation (SIMT) [21] including stacking faults, might occur by plastic deformation during wear. According to Eq. (2), the volume fractions of the $\gamma \rightarrow \varepsilon$ phase on the discs′ surfaces were estimated to be 17% and 4% for LC and HC alloys, respectively.

Table 4
Results of composition at numbered points by EPMA analyses.

Point		Co	Cr	Mo	C	Si	Mn
LC	1	64.16	29.239	6.476	0.279	0.798	0.675
	2	48.382	35.199	15.931	0.263	1.049	0.641
HC	1	65.399	27.347	6.614	0.579	0.654	0.714
	2	32.491	22.983	39.778	1.862	2.897	0.277
	3	16.315	66.505	12.27	3.801	0.016	0.565

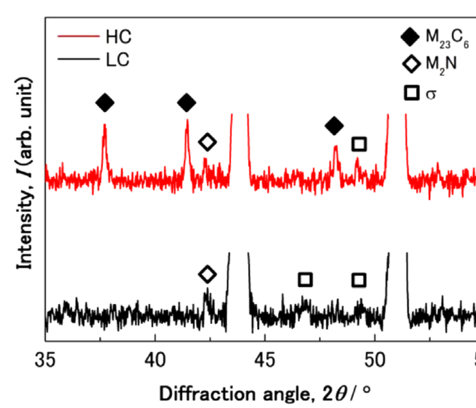

Fig. 4. Results of elaborated X-ray profiles showing second phase precipitates of σ phase, M_2N in LC alloy, and σ phase, M_2N and $M_{23}C_6$ in HC alloy.

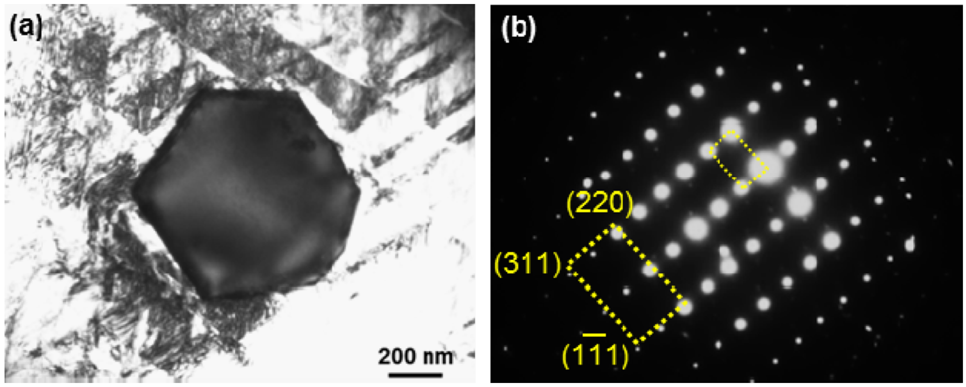

Fig. 5. TEM micrographs of (a) eutectic $M_{23}C_6$ precipitated in HC matrix and (b) diffraction pattern.

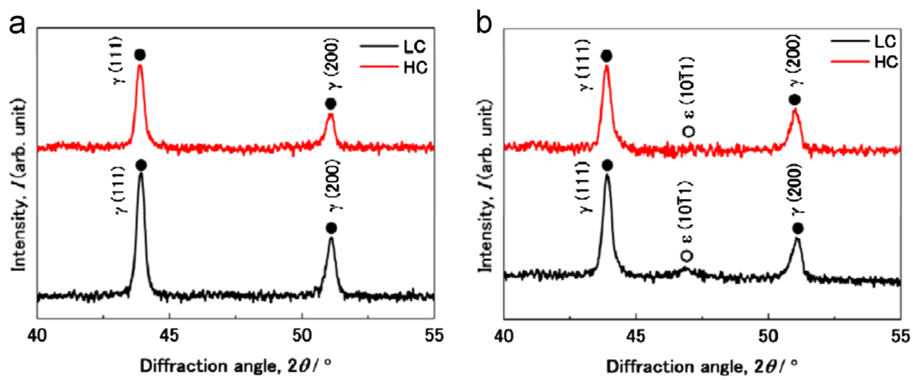

Fig. 6. X-ray profiles of LC and HC alloys under (a) as-polished and (b) worn conditions, indicating slight increase in the peak intensity of ε phase after wear.

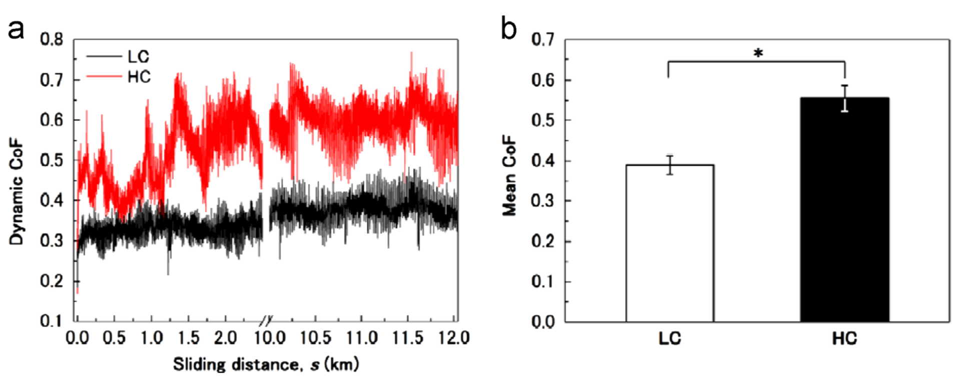

Fig. 7. (a) Dynamic and (b) mean CoFs for LC and HC alloys under a constant 9.8 N load in Hanks′ solution, in which LC endured lower CoF with less “noisy”. Asterisks denote significant differences for mean CoFs of LC and HC alloys according to the Student′s t-test with $P<0.05$, and error bars denote the mean ± standard deviation.

3.2. Wear behavior

3.2.1. Coefficient of friction

Fig. 7(a) and (b) shows the dynamic and mean coefficients of friction (CoFs) of LC and HC alloys under a constant 9.8 N load. The dynamic CoFs had steep slopes for the first 0.1 km, and then gentle increases in the subsequent stage for both samples. These changes in the CoF reflect the initial run-in stage followed by a relatively steady phase, a common transition for friction pairs and are usually attributed to changes in the nature of the contact and frictional heating in local areas [22,23]. The statistical significance of the CoF determined by the Student′s t-test (assuming unequal variances; two-tail, $P<0.05$) indicated that the LC and HC alloys exhibited significantly different stable CoFs, which were observed to be 0.39 and 0.52, respectively. The LC alloy exhibited lower CoF with less “noisy”, so it endured less

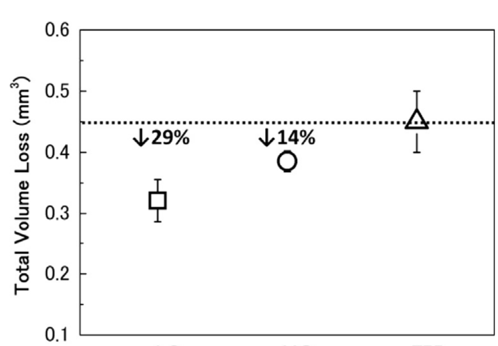

Fig. 8. Total volume loss of the LC, HC, and ASTM F75 alloys after wear tests with their error bars (standard deviation). LC alloy had better wear resistance than the other alloys.

tangential friction and exhibited smoother contact than the HC alloy during wear test.

3.2.2. Volume loss and wear factor

Fig. 8 shows that the total volume losses are 0.32 mm^3 and 0.39 mm^3 for LC and HC bearings, respectively. They decreased 29% and 14% compared to that of the commercial cast ASTM F75 alloy under the same experimental conditions [14]. The results illustrate that the wrought alloys used in present study exhibited better wear resistance than the cast one, especially for the LC alloy.

Fig. 9 shows the total wear factors ($\times 10^{-7}$ mm^3/N m) of LC and HC alloys, which in accordance with the total volume losses. Pins experienced lower wear factors than the corresponding discs for both LC and HC alloys. According to Student's *t*-test (assuming unequal variances; two-tail, $P<0.05$), no significant difference was observed between the wear factors of the LC and HC pins; but significant difference was found between that of the discs, indicating obviously higher wear factors of HC disc than that of LC one.

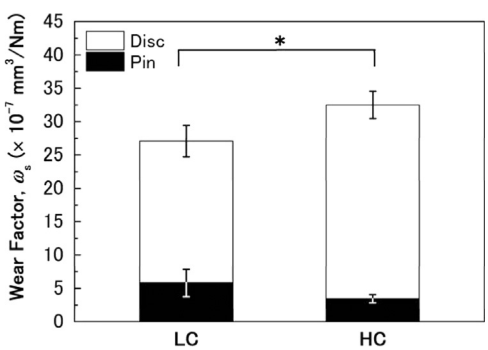

Fig. 9. Wear factors of pins and discs for LC and HC alloys. Asterisks denote significant differences for the wear factors of the discs according to Student's *t*-test with $P<0.05$, and error bars denote the mean ± standard deviation.

3.2.3. Surface topography

The laser and 3D micrographs of the wear tracks on LC and HC discs are shown in Fig. 10(a and b) and (c and d), respectively, and that of worn surface topographies on LC and HC pins shown in Fig. 11(a and b) and (c and d), in which the relative sliding directions of the counter bodies are indicated by white arrows. All the results depict obvious stripe wear on both LC and HC worn surfaces. The HC discs exhibited ~4 μm deeper wear tracks than that on the LC ones, whereas the HC pins were ~3 μm deeper.

Detailed compositional images in Fig. 12(a and b) show some evident abrasions on the worn surface of LC and HC discs, respectively. These abrasion were characterized by scratches and grooves parallel to the sliding direction [24,25], with widths in range of ~0.1–2 μm. Many bright particles, considered as σ-phase precipitates, were observed residual at the ends of some scratches. They were inferred to be partially fractured during wear and bring about the consequent abrasions. Some of them were completely torn off, for the positions they occupied were substituted by holes on the grooves. In contrast to abrasions generated by micro plowing or micro cutting of σ-phase precipitates [26], multiple micro cracks were also observed scattered in vicinity of some dark pitting in dotted white circles as shown in Fig. 12(c), and the latter feature was considered as torn off carbides on the worn HC surface.

Compared to the dominant abrasion and pitting on discs' wear tracks, the SEM micrographs in Fig. 13 depict mixed abrasion, micro pitting (surface delaminations) and adhesion for both LC (a–c) and HC (d–f) pins. LC pins have relatively separated stripe zones indicating abrasion and micro pitting parallel to the sliding direction, and the later feature may form under the cyclic stress. In contrast, a severe pitting-groove-mingled surface similar micro cracks on discs were observed on the worn surfaces of HC pins.

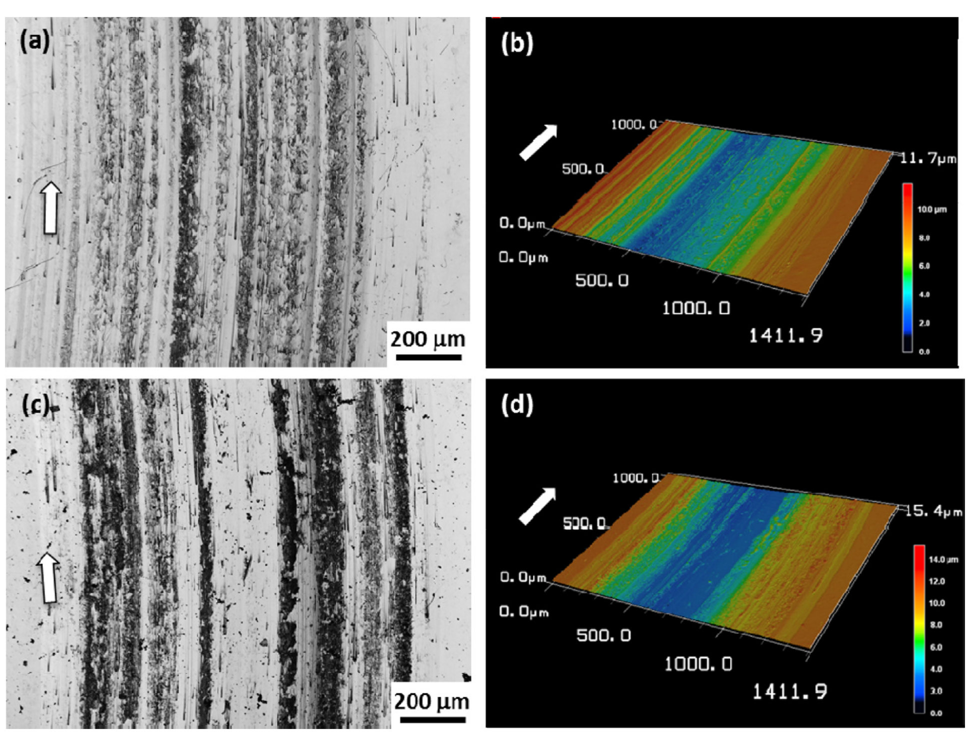

Fig. 10. The laser and 3D micrographs of the wear tracks on ((a) and (b)) LC and ((c) and (d)) HC discs, in which the sliding directions are indicated by white arrows. HC wear track shows deeper wear depth.

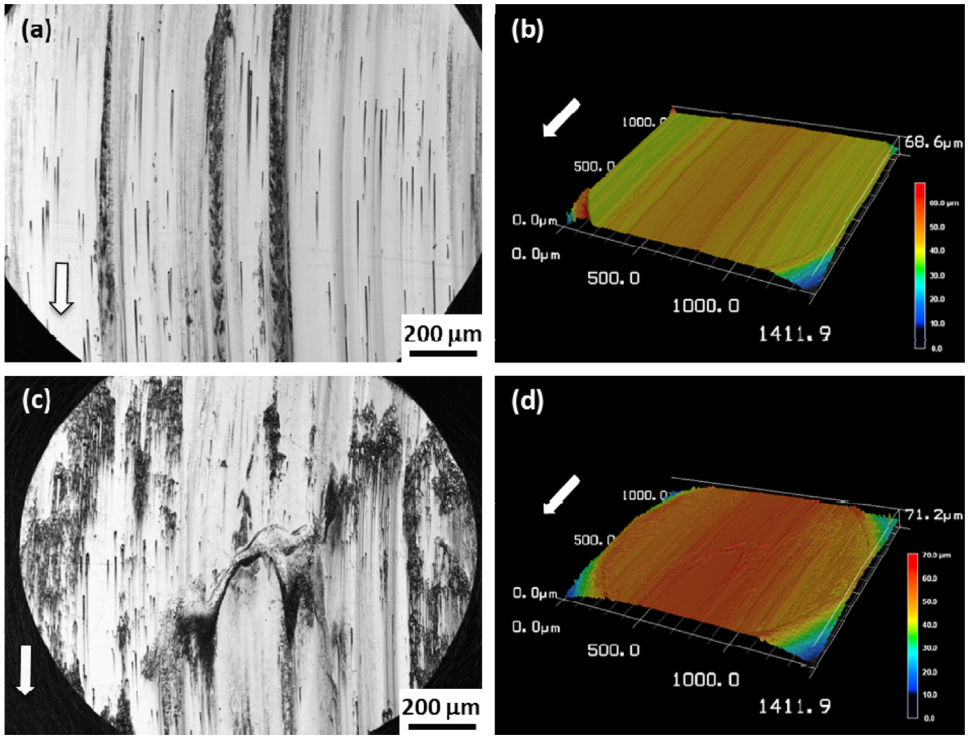

Fig. 11. LM micrographs and 3D images of the worn surface topography on ((a) and (b)) LC and ((c) and (d)) HC pins, in which the sliding directions are indicated by white arrows. HC pin shows deeper fall of surface topography.

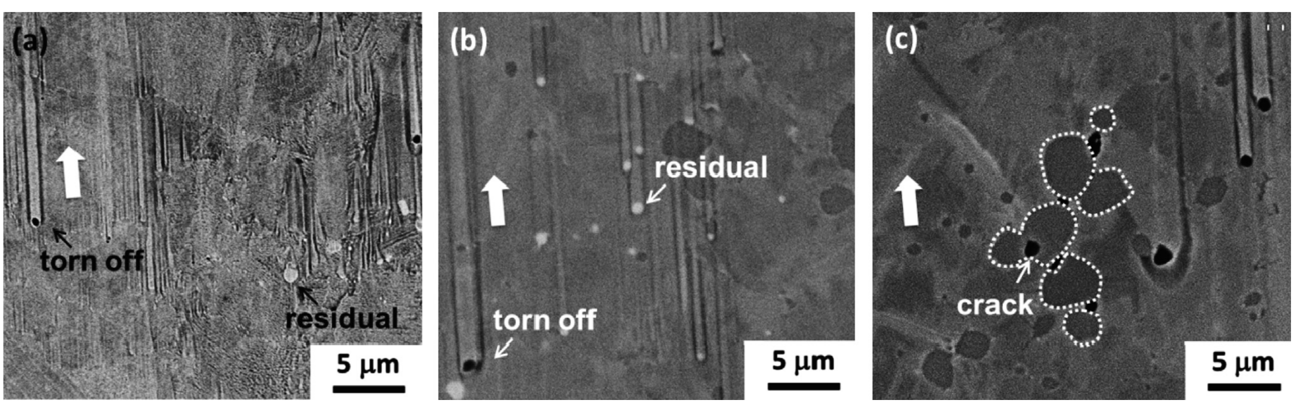

Fig. 12. Detailed compositional images indicating typical surface topographies including (a) obvious abrasion on LC worn surface, and both (b) abrasion and (c) micro cracks between dark pitting encircled in dotted white circles of HC worn surface.

These grooves are more concentrated, short, interlacing with torn-off-carbide-induced pitting, micro cracks manifesting as black holes, or residual precipitates of carbides/σ phase.

3.3. Surface roughness

The arithmetic average roughness (*Ra*) and 10-point mean roughness (*Rz*) of the as-polished and worn surfaces of LC and HC samples are listed in Table 5.

Before the wear test, the *Ra* values were ~6 nm and 10 nm for the LC and HC discs, respectively. A Student's *t*-test (assuming unequal variances; two-tail, $P<0.05$) revealed that *Ra* values for the alloys had significant differences from each other, since the HC alloy had larger precipitates protuberating from its matrix. In contrast, the LC alloy, with smaller and fewer precipitates, showed a lower *Ra*, a lower CoF and less friction during lubricated sliding wear [36]. The worn surface topographies were characterized by abrasions, cracks, and consequently the *Ra* values were found to be increased to ~0.03 µm for both LC and HC worn surfaces.

In contrast, pins with spherical tips have similar initial larger *Ra* values for both LC and HC alloys, between which no significant difference was observed by Student's *t*-test (assuming unequal variances; two-tail, $P<0.05$). Their *Ra* values rose significantly after wear, especially for the HC pins, with severe pitting-groove-mingled worn surface and more adhering Ca–PO_4 compounds (Fig. 13).

The cross-sectional wear track profiles for the LC and HC alloys are shown in Fig. 14(a) and (b). The HC alloy had notably wider and deeper cross-sectional wear track profiles; in contrast, the LC alloy showed narrower and shallower ones. The volume loss could be roughly estimated according to the wear track profiles of disc and laser micrographs of worn zone of pin, as shown in Fig. 15. The results are in good agreement with that obtained from the tests (Fig. 8), indicating that the LC discs wore less, while the HC pins wore less.

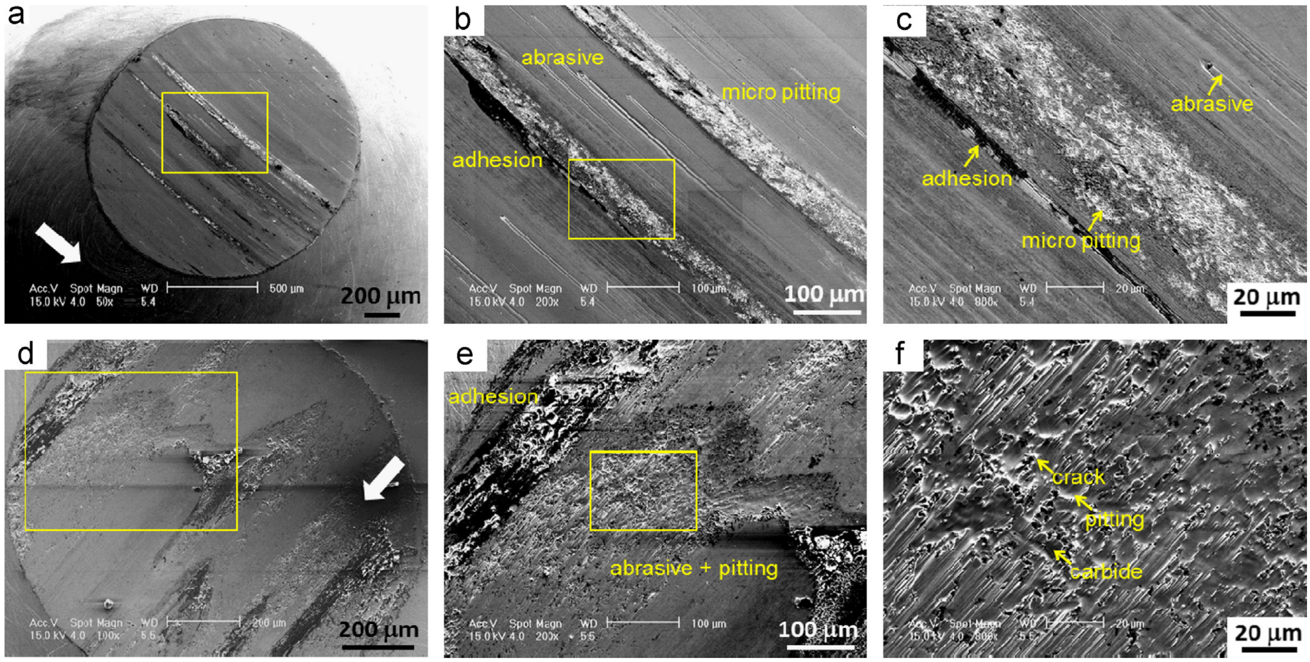

Fig. 13. Detailed SEM micrographs of worn (a)–(c) LC, and (d)–(e) HC pins, in which LC alloy shows abrasion, micro pitting (surface delamination) and adhesion, and HC one shows abrasion, pitting and cracks, adhesion.

Table 5
Surface roughness of as-polished and worn LC and HC discs, with 8 measurements by stylus profilometer; and that of as-polished and worn LC and HC pins, with 3 measurements by LM.

		Disc (line: 3 mm)		Pin (area: 26.709 µm^2)	
		Ra (µm)	*Rz* (µm)	*Ra* (µm)	*Rz* (µm)
As-polished surf.	LC	0.006 ± 0.001	0.049 ± 0.001	0.018 ± 0.001	0.132 ± 0.008
	HC	0.010 ± 0.002	0.102 ± 0.043	0.019 ± 0.001	0.160 ± 0.009
Worn surf.	LC	0.030 ± 0.001	0.136 ± 0.025	0.477 ± 0.224	5.618 ± 1.691
	HC	0.029 ± 0.001	0.128 ± 0.034	0.704 ± 0.307	10.450 ± 4.697

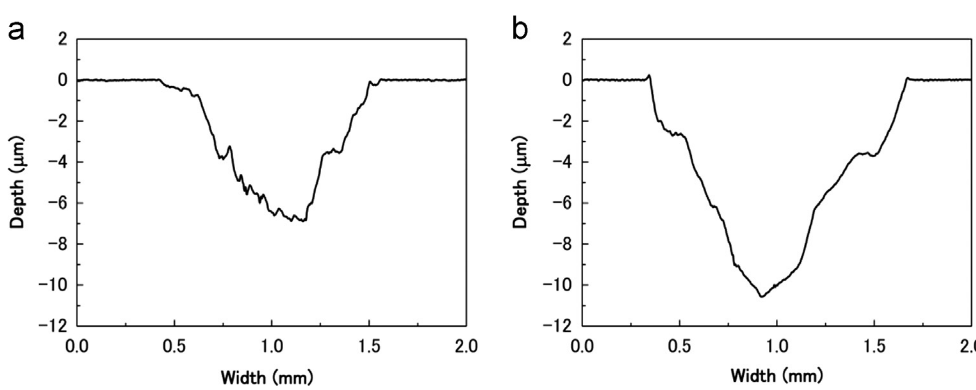

Fig. 14. Wear track profiles (cross-section) of (a) LC and (b) HC alloys after the wear test, indicating narrower and shallower wear track of LC alloy.

3.4. Vickers hardness

Fig. 16(a) and (b) shows the Vickers hardness of the as-polished and worn surfaces on the discs obtained using 1 N and 0.05 N loads, respectively. These values are assumed to represent the macro and micro scale hardness underneath the worn surfaces, as the indention depths could be calculated as ~3 µm and 600 nm for HV1 and HV0.05, respectively. It was found that the as-polished HC surface was harder than the LC surface because of the strengthening effect of the larger amount of precipitates. After the wear test, hardness increases were observed for both alloys. However, the increment in HV0.05 for the LC alloy was ~100, about twice that for the HC alloy, which indicates that the LC alloy exhibited a stronger hardening effect at the worn surface below the indent depth of 570 nm.

TEM images of the worn surface cross-sections are shown in Fig. 17, in which some striations beneath the LC worn surface can be observed in the dark-field image (Fig. 17(a)). The orientation relationship with the matrix is in accordance with the Shoji–Nishiyama relation (S–N relation) [27,28] (see Fig. 17(a'))

$$(1\ 1\ 1)_{fcc} \parallel (0\ 0\ 0\ 1)_{hcp}$$

Therefore, these striations were conformed to be strain-induced martensite (SIM), which can also be observed by XRD profiles in Fig. 6. The SIM gave rise to a noticeable increase in the hardness and wear resistance for the LC alloy [29,30]. However, Fig. 17(b) shows no obvious SIM beneath the worn HC surface.

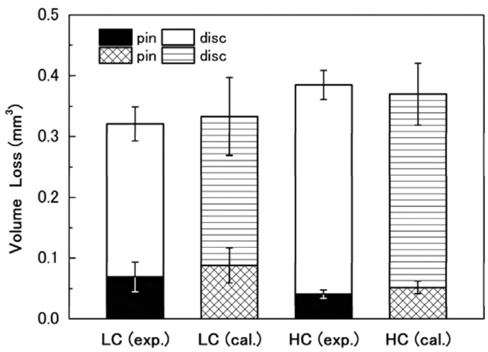

Fig. 15. Volume loss of LC and HC alloys obtained from experimental and calculated results.

4. Discussion

In this study, microstructure is proved to affect the CoCrMo alloys wear behavior significantly. Different volume loss amounts, surface topographies and wear mechanisms were obtained for LC and HC alloys, because that different carbon contents lead to different properties of, and precipitates in the matrix.

The CoFs were comparable to those observed by other workers under similar saline lubrication [7,14]. For all the samples the dynamic CoFs were increased gradually with prolonged sliding distance, as they had a steep slope for the first 0.1 km. The CoF of HC alloy increased more and fluctuated more violently than that of LC one, owing to harder precipitates and rougher surfaces of the HC alloy. As a result of low-viscosity Hanks′ lubrication [31–33] and low sliding speed of the disc [13], the lubricant film thickness in the present study was considered to be insufficient to bear the load, and main contact between surfaces is considered to be (1) precipitate/precipitate contact; or (2) precipitate/matrix contact when the pin and disc just contact with each other. The initial contact pressure between precipitates would be considerably higher than 1.7 GPa by Hertz contact theory [17], even exceed the hardness of the precipitates, ~11 GPa and 15 GPa for the σ

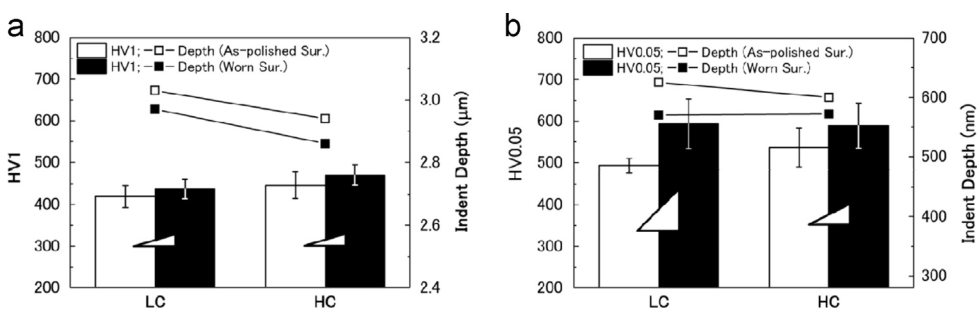

Fig. 16. Vickers hardness and indent depths of (a) HV1 and (b) HV0.05 on the as-polished and worn LC and HC surfaces, indicating stronger hardening effect at the worn surface of LC alloy below the indent depth of 570 nm.

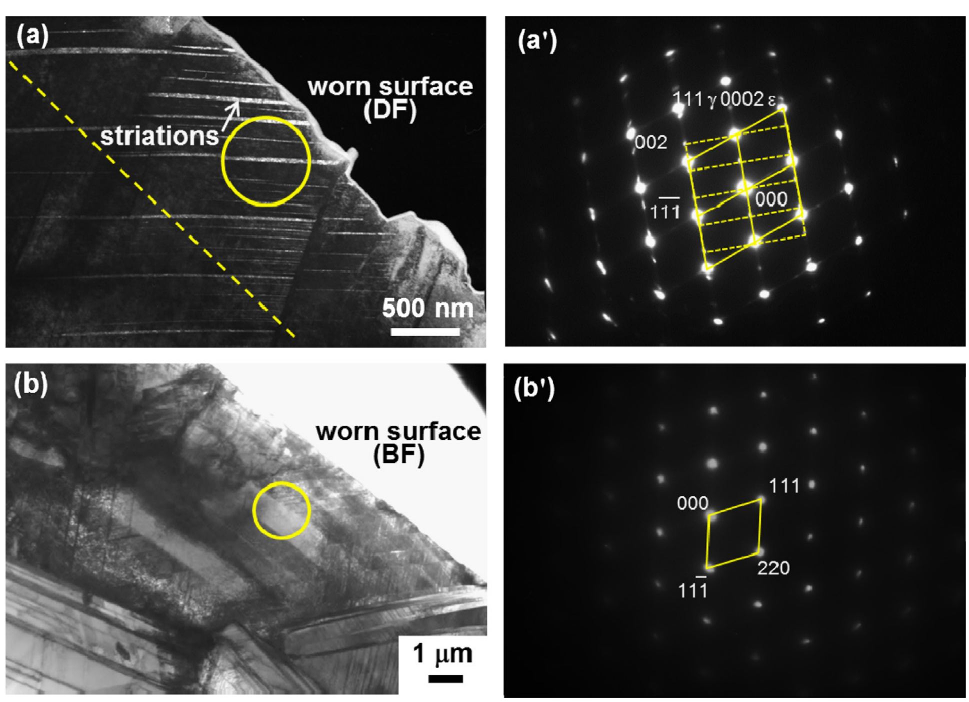

Fig. 17. (a) Dark-field TEM images of worn surfaces and (a′) diffraction pattern of the LC alloy, and (b) bright-field TEM images of worn surfaces and (b′) diffraction pattern of the HC alloy.

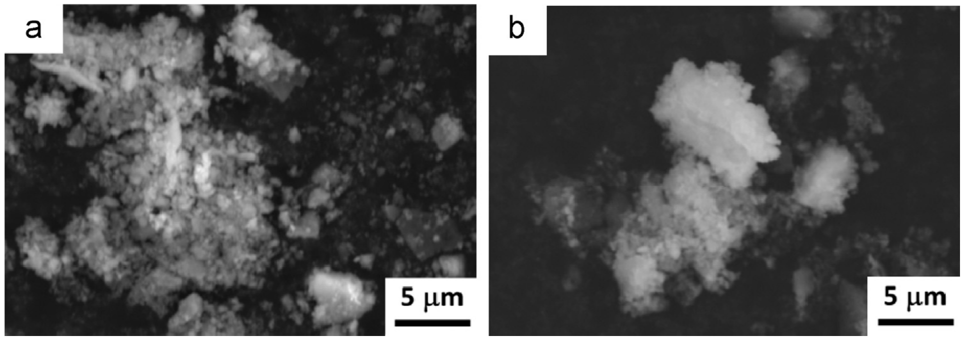

Fig. 18. SEM micrographs of the wear debris generated in Hanks′ solution for (a) LC and (b) HC alloys.

Table 6
Wear rates (nm/min) of LC and HC specimen estimated from (a) volume loss and (b) worn surface topography.

	(a)	(b)
LC pin	9.52	10.71
HC pin	7.34	8.33
LC disc	0.99	0.97
HC disc	1.36	1.26

phase and $M_{23}C_6$ carbide, respectively [13,34]. Hard precipitates would fracture, or be torn off from the matrix, to form debris that either be embedded in the matrix or roll between the matrix surfaces [35]. Fig. 18 shows the SEM micrographs of the (a) LC and (b) HC wear debris, respectively. Despite that they agglomerated together, the HC debris, possibly including some larger precipitates, are larger in size than the LC ones, then lead to a higher, unstable CoF of HC alloy (Fig. 7). Meanwhile, segregation of carbides on the discs and the drastic deterioration of the pin surface topography may also be relevant to the high CoF of the HC alloy. In opposite, the LC alloy exhibited a relative lower, stable CoF which should be attribute to the unobvious precipitates and the generation of SIM structure [7].

The volume losses and the wear factors for the two alloys diminished noticeably compared to that of the commercial cast ASTM F75 alloy, especially for LC alloy, under the same experimental conditions. However, the wear factor of LC alloy (with ave. grain size of ~20 μm) is observed to be larger than that of the same low carbon forged CoCr alloy (with ave. grain size of ~11 μm) [14]. Tipper et al. also mentioned that grain size is a significant factor to determine the wear resistance [12], and may contribute to the constant inconsistent disputes between whether carbide (with various kind, distribution, fraction and morphology) contribute to improving the wear resistance or not [8–14]. However, for the LC and HC alloys with similar grain size in this study, the former was observed better wear resistance by judging from the total volume loss and wear factor.

It is remarkable that similar less wear factors of pin than that of disc could be observed for the like–like tests conducted under saline solution lubricated environment [14,12], whereas the rule is not apply to these conducted in diluted bovine serum, in which wear factors of pins and discs exhibited no regularity [11,12]. In the present study, the wear factors of pin experience only 21.5% and 10.7% of the total wear factors for the LC and HC alloy, respectively. We can roughly estimate the wear rates (in nm/min) of pins and discs by estimation from volume loss or the surface topographies as shown in Table 6, with the simplification that worn shape of pin is spherical crown, and the crosssection profile of wear track is triangle. The results obtained by the two methods resembled each other. Wear rates of pin are strikingly higher than that of disc, ~10 and 6 time folder for the LC and HC alloy, respectively. The reason for the asymmetric wear rates comes from different sliding distance and temperature for the pins and discs. The discs, whose contact distribute along the rotation circle (ϕ 16 mm), had relatively less sliding distance and elevation in temperature for every grain in the matrix during wear [13], consequently the corresponding low wear rate and wear factor within the mild-sliding wear. It should be noted that these wear rate values are assumed to be calculated by fixed worn areas measured at the end of test, but actually the wear rates changed dynamically from run-in to steady mild wear.

The LC discs resisted better with lower wear rate, which resembled with surface damage after wear tests in Figs. 10 and 14. The cross-sectional wear track on the LC surface indicates a more steady wearing away of the material [36]. We can compare quantitative surface topographies and height images in Fig. 19(a)–(c), and (d)–(f) on the LC and HC worn discs, respectively, by LM. Abrasion in (a) and abrasion and micro cracks in (d) was observed as mentioned in Section 3.2.3, indicating the weak constituents of these alloys. Previous studies by Bina et al. revealed that brittle precipitations of the σ phase, with a low fracture toughness, tend to precipitate incoherently at boundaries and be fractured as high contact pressure was exerted on them [37–41]. Therefore, the σ-phase precipitates, preferring along grain boundaries (GB) in LC alloy, were frequently observed to be partially fractured, and dug out into the matrix of counter body to form sizable scratches and grooves during wear. Most of them left their residual parts at the ends of abrasion, which indicates two-body abrasive wear; while minority were completely torn off from the matrix to bring about three-body wear (Fig. 12) [7,42]. The height image (Fig. 19(b)) of LC worn surface topography was composed of grain basins of the lower penetrated matrix surrounded by higher residual sticking σ precipitates along GB, which indicates LC alloy was dominated by two-body abrasive wear.

Both σ-phase and carbide precipitates participated in the wear process, collectively and interactively, which made wear behavior of HC alloy more complicated. Initial contact in HC alloy is speculated to be prevailed by semicoherent carbide/carbide contact because they were larger and trend to protrude from the matrix. Many carbide precipitates were torn off from the matrix preferentially owing to the high initial contact pressure they bore, as shown by some traces of pitting indicated in dotted circles in Fig. 12(c) and Fig. 19(e). These hard debris of detached carbides would impact between the surfaces or roll around freely, then cause three-body wear and surface fatigue during a short period run-in phase, similar to that depicted by Wimmer et al. [13,7].

In HC alloy, plenty of σ-phase precipitates have also been observed at carbide/carbide boundaries (Fig. 3). These precipitates around carbides corners tended to be particularly weak as carbides in vicinity are torn off, since they are exposed to contact with each other by no protection and firm support. They would be uprooted from the embrittled boundaries of the matrix [43], and evolve into

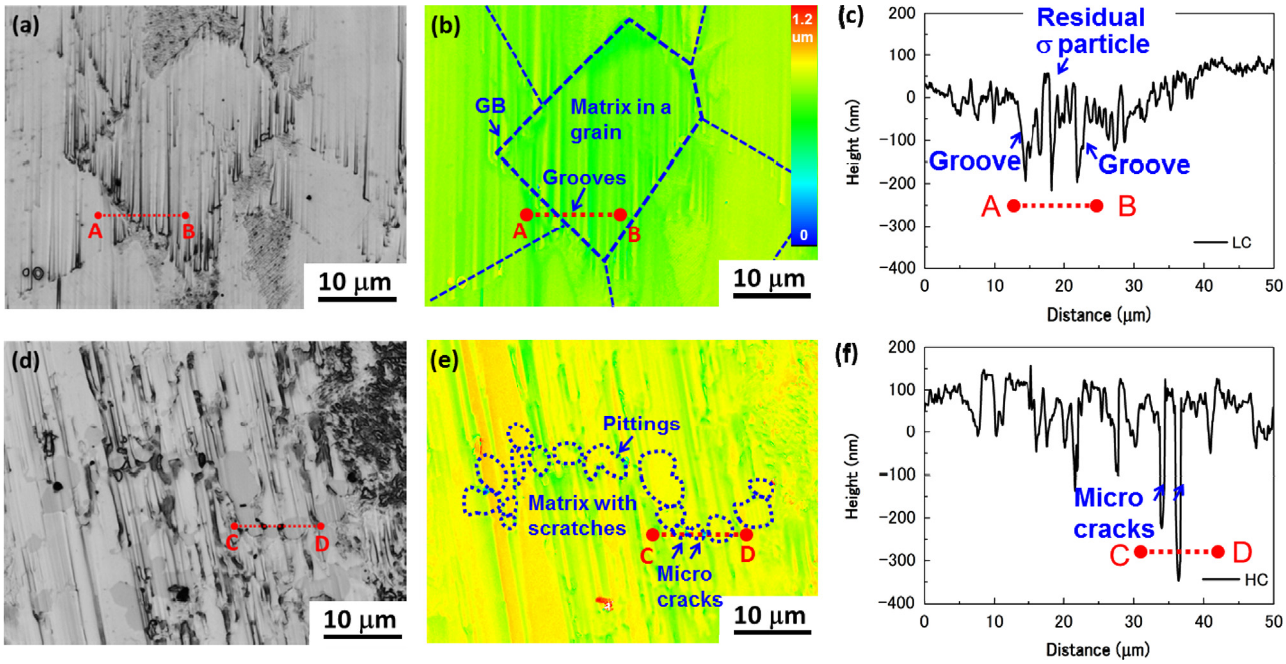

Fig. 19. LM images of the surface topographies on wear tracks of (a)–(c) LC and (d)–(e) HC alloys, in which (c) and (f) show typical size of abrasion between lined AB interval on LC surface and micro cracks between lined CD interval on HC surface, respectively.

surface fatigue in the form of intergranular micro cracks [44]. Fig. 19(c) and (f) shows worn surface topographies and sizes of typical abrasion on LC and micro crack on HC in lined AB and CD intervals, in which typical micro cracks was observed to propagate into a depth of ~0.3–0.4 μm, deeper than the depth of scratches and grooves of ~0.1–0.2 μm. Therefore, compared to the dominant two-body abrasion for LC alloy with grain basins, we deduce that the coexistence of σ-phase and carbide particles would bring about synergy effects for surface fatigue and three-body abrasion with wider and deeper grooves, which was considered to be the dominant wear mechanisms for HC alloy.

We also found that despite of the less volume loss, the pins experienced much more wear rates than the discs. The worn surface topography of pins (Fig. 13) exhibits similar and common features to that of disc. Grooves of ~0.1–2 μm wide were observed on both LC and HC pins, despite that on the HC surface were shorter, and more intensive as they were cut off by the residual carbides or pitting. Also surface fatigue, characterized by carbide-torn-off-induced-pitting and cracks are observed on the HC pin. Areas of adhesion, revealing high concentrations of lubricant component, were observed entrapped within the abrasion. Micro pitting were observed in stripe zones on LC pins, similar to that reported by Hernández-Rodríguez et al. [45], who used cast CoCrMo with globular carbides of M_6C in 2–10 μm under bovine serum lubrication. The worn topography indicates that micro pitting could be due to debris detached from matrix where no precipitates exist by cyclic contact, but with little relevance of torn-off precipitates and the lubricant applied. We deduce the micro pitting generation is also related to temperature elevation because such defect was not observed on the counter LC discs. Pitting formation can accelerate the wear rate, and make unconspicuous difference between wear behavior of both LC and HC pins.

It is worth mentioning that γ FCC matrix is metastable, and is kinetically favored due to the sluggishness of the FCC to HCP transformation by adding other elements such as C and N [46–48]. Lattice defects like twins and stacking faults induced into ε-phase martensite, which was observed in a plastically deformed layer of ~600 nm beneath the worn LC disc as shown in Fig. 17

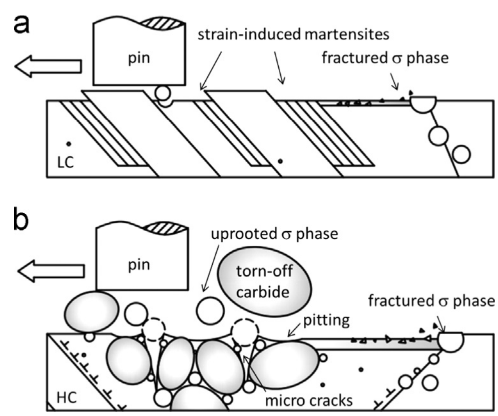

Fig. 20. Wear mechanisms for (a) LC and (b) HC alloy.

(a) [49], results in obvious increased work hardening effect (Fig. 16), therefore the enhanced wear resistance of LC surface. However, little strain-induced martensite was observed on the HC worn surface, since carbon addition can increase the stacking fault energy significantly and decrease the density of stacking faults, twins and martensite [50,51], which is similar to the previous results depicted by Saldívar-García et al. [47].

In summary, the HC alloy would be worn more seriously because it exhibited carbide-torn-off-induced surface fatigue and three-body abrasive wear caused by strong interaction between the σ-phase and carbide precipitates. In contrast, the LC alloy exhibited relatively mild two-body abrasive wear because less σ-phase precipitates in its initial microstructure and more SIM in its worn microstructure were observed. The wear mechanisms of both LC and HC alloys are summarized in Fig. 20(a) and (b), respectively, and it is deduced that the dominant wear mechanism for the LC alloy was fractured and torn-off σ induced abrasion; whereas the torn-off carbides and σ particles in vicinity promoted surface fatigue, which was considered as one of the most dominant wear mechanism for the HC alloy.

5. Conclusions

In the present study, the synergy effects of the σ phase and carbide on the wear behavior of CoCrMo alloys under Hanks′ lubricated condition has been evaluated. The following conclusions can be drawn from this study:

(1) The HC bearings, owing to harder precipitates and rougher surfaces, exhibited higher CoF than the LC ones.
(2) The LC bearings resisted better than the HC ones with less wear factor. Worn surface topographies were characterized by scratched grain basins with raised σ-phase precipitates along GB for the LC alloy, whereas mixed abrasion, pitting and cracks for the HC alloy.
(3) The LC disc showed a significantly less wear than the HC one, since the former is dominated by fractured-σ-phase-induced two-body abrasive wear, whereas the latter by precipitate-torn-off-induced surface fatigue and three-body abrasive wear.
(4) Strain-induced martensite observed on the worn surface of LC disc was contributed to the increase of hardness and abrasion resistance.
(5) Surface fatigue of micro pitting made no significant difference in wear factor of LC and HC pins.
(6) The microstructure of the σ-phase and carbide precipitate combination is detrimental to the CoCrMo wear behavior.

Acknowledgements

The authors gratefully acknowledge the financial support of the Ministry of Education, Culture, Sports, Science and Technology of Japan, as part of the Regional Innovation Cluster Program 2010. The authors also acknowledge I. Narida, Y. Kodama and S. Ito for assistance with the EPMA, FIB and TEM assistance, respectively.

References

[1] W. Betterridge, Cobalt and its Alloys, Halsted Press, Chichester, 1982.
[2] A. Buford, T. Goswami, Review of wear mechanisms in hip implants: I—General, Mater. Des. 25 (2004) 385–393.
[3] D.J. Langton, S.S. Jameson, T.J. Joyce, N.J. Hallab, S. Natu, A.V.F. Nargol, Early failure of metal-on-metal bearings in hip resurfacing and large-diameter total hip replacement: a consequence of excess wear, J. Bone Joint Surg. Br. 92-1 (2010) 38–46.
[4] M. Bryant, M. Ward, R. Farrar, R. Freeman, K. Brummitt, J. Nolan, A. Neville, Failure analysis of cemented metal-on-metal total hip replacements from a single centre cohort, Wear 301 (2013) 226–233.
[5] J.C. Walker, R.B. Cook, J.W. Murray, A.T. Clare, Pulsed electron beam surface melting of CoCrMo alloy for biomedical applications, Wear 301 (2013) 250–256.
[6] J.R. Davis, ASM Specialty Handbook: Nickel, Cobalt, and Their Alloys, ASM International, Materials Park, OH, 2007.
[7] Y. Bedolla-Gil, M.A.L. Hernandez-Rodriguez, Tribological behavior of a heat-treated cobalt-based alloy, J. Mater. Eng. Perform. 22 (2013) 541–547.
[8] J.K. Fulcher, T.H. Kosel, N.F. Fiore, The effect of carbide volume fraction on the low stress abrasion resistance of high Cr–Mo white cast irons, Wear 84 (1983) 313–325.
[9] V.M. Desai, C.M. Rao, T.H. Kosel, N.F. Fiore, Effect of carbide size on the abrasion of cobalt-base powder metallurgy alloys, Wear 94 (1984) 89–101.
[10] J. Cawley, J.E.P. Metcalf, A.H. Jones, T.J. Band, D.S. Skupien, A tribological study of cobalt chromium molybdenum alloys used in metal-on-metal resurfacing hip arthroplasty, Wear 255 (2003) 999–1006.
[11] S.C. Scholes, A. Unsworth, Pin-on-plate studies on the effect of rotation on the wear of metal-on-metal samples, J. Mater. Sci.: Mater. Med. 12 (2001) 299–303.
[12] J.L. Tipper, P.J. Firkins, E. Ingham, J. Fisher, M.H. Stone, R. Farrar, Quantitative analysis of the wear and wear debris from low and high carbon content Co–Cr alloys used in metal-on-metal total hip replacements, J. Mater. Sci.: Mater. Med. 10 (1999) 353–362.
[13] M.A. Wimmer, J. Loos, R. Nassutt, M. Heitkemper, A. Fischer., The acting wear mechanisms on metal-on-metal hip joint bearings: in vitro results, Wear 250 (2001) 129–139.
[14] A. Chiba, K. Kumagai, N. Nomura, S. Miyakawa, Pin on disk wear behavior in a like-on-like configuration in a biological environment of high carbon cast and low carbon forged Co–29Cr–6Mo alloys, Acta Mater. 55 (2007) 1309–1318.
[15] Y. Yamashita, Y.P. Li, E. Onodera, H. Matsumoto, A. Chiba, Dynamic recrystallization behavior of biomedical CCM alloy with additions of C and N, Mater. Trans. 51 (2010) 1633–1639.
[16] K. Yamanaka, M. Mori, A. Chiba, Nanoarchitectured Co–Cr–Mo orthopedic implant alloys: nitrogen-enhanced nanostructural evolution and its effect on phase stability, Acta Biomater. 9 (2013) 6259–6267.
[17] H.R. Hertz, Über die Berührung fester elastischer Körper und über die Härte, Sitzungsbericht des Vereins zur Förderung des Gewerbefleiβes (1882) 449–463.
[18] J. Fisher, D. Dowson, Tribology of total artificial joints, Proc. Inst. Mech. Eng. Part H J. Eng. Med. 205 (1991) 73–79.
[19] M. Sage, Ch. Guillaud, Revue de Metallugie, XLVII, Siderurgy Research Institute (I.R.S.I.D.) (1950) 139–145.
[20] S. Kurosu, Hiroaki Matsumoto, Akihiko Chiba, Grain refinement of biomedical Co–27Cr–5Mo–0.16N alloy by reverse transformation, Mater. Lett. 64 (2010) 49–52.
[21] K. Yoda, Suyalatu, A. Takaichi, N. Nomura, Y. Tsutsumi, H. Doi, S. Kurosu, A. Chiba, Y. Igarashi, T. Hanaw, Effects of chromium and nitrogen content on the microstructures and mechanical properties of as-cast CoCrMo alloys for dental applications, Acta Biomater. 8 (2012) 2856–2862.
[22] B. Patel, G. Favaro, F. Inam, M.J. Reece, A. Angadji, W. Bonfield, J. Huang, M. Edirisinghe, Cobalt-based orthopaedic alloys: relationship between forming route, microstructure and tribological performance, Mater. Sci. Eng., C 32 (2012) 1222–1229.
[23] S. Mischler, A.I. Muñoz, Wear of CoCrMo alloys used in metal-on-metal hip joints: a tribocorrosion appraisal, Wear 297 (2013) 1081–1094.
[24] H.G. Willert, G.H. Buchhorn, D. Göbel, G. Köster, S. Schaffner, R. Schenk, M. Semlitsch, Wear behavior and histopathology of classic cemented metal on metal hip protheseses, Clin. Orthop. 32 (1996) 160–186.
[25] F.W. Chan, J.D. Bobyn, J.B. Medley, J.J. Krygier, M. Tanzer, Wear and lubrication of metal-on-metal hip implants, Clin. Orthop. 369 (1999) 10–24.
[26] R. Büscher, G. Täger, W. Dudzinski, B. Gleising, M.A. Wimmer, A. Fischer, Subsurface microstructure of metal-on-metal hip joints and its relationship to wear particle generation, J. Biomed. Mater. Res. 72B (1) (2004) 206–214.
[27] Z. Nishiyama, Martensite Transformation, Academic, New York, 1978.
[28] L. Remy, Kinetics of strain-induced fcc→hcp martensitic transformation, Metall. Trans. A 8A (1977) 253–258.
[29] L. Remy, A. Pineau, Twinning and strain-induced F.C.C.–H.C.P. transformation on the mechanical properties of Co–Ni–Cr–Mo alloys, Mater. Sci. Eng 26 (1976) 123–132.
[30] Y. Koizumi, S. Suzuki, K. Yamanaka, B.S. Lee, K. Sato, Y.P. Li, S. Kurosu, H. Matsumoto, A. Chiba, Strain-induced martensitic transformation near twin boundaries in a biomedical Co–Cr–Mo alloy with negative stacking fault energy, Acta Mater. 61 (2013) 1648–1661.
[31] J.B. Medley, J.J. Krygier, J.D. Bobyn, F.W. Chan, A. Lippincott, M. Tanzer, Kinematics of the MATCO@ hip simulator and issues related to wear testing of metal–metal implants, Proc. Inst. Mech. Eng. Part H J. Eng. Med. 211 (1997) 89–99.
[32] G.W. Stachowiak, A.W. Batchelor, Physical properties of lubricants, in: Tribology Series, 24, Engineer Tribology, Elsevier Science Publishers B.V. 24 (1993).
[33] J. Kestin, H.E. Khalifa, R.J. Correia, Tables of the dynamic and kinematic viscosity of aqueous NaCl solutions in the temperature range 20–150 °C and the pressure range 0.1–35 MPa,, J. Phys. Chem. Ref. Data 10 (1981) 57–70.
[34] The Japan Institute of Metals and Material, The Data Book for the Metals, third ed., Maruzen, Tokyo (1993) 159–163.
[35] K.-H. Zum Gahr, Microstructure and Wear of Materials, Elsevier, New York, 1987.
[36] M. Sedlaček, B. Podgornik, J. Vižintin, Correlation between standard roughness parameters skewness and kurtosis and tribological behavior of contact surfaces, Tribol. Int. 48 (2012) 102–112.
[37] M.H. Bina, Homogenization heat treatment to reduce the failure of heat resistant steel castings, in: Y. Pardhi (Ed.), Metallurgy—Advances in Materials and Processes, InTech, New York, 2012. (chap. 5).
[38] M. Pohl, O. Storz, T. Glogowski, Effect of intermetallic precipitations on the properties of duplex stainless steel, Mater. Charact. 58 (2007) 65–71.
[39] L. Karlsson, L. Bengtsson, U. Rolander, S. Pak, Proceedings of the Applications of Stainless Steel, Stockholm, Sweden, 1992, pp. 335–344.
[40] C.C. Hsieh, D.Y. Lin, T.C. Chang, Microstructural evolution during the δ/σ/γ phase transformation of the SUS 309L Si stainless steel after aging under various nitrogen atmospheric ratios, Mater. Sci. Eng., A 475 (2008) 128–135.
[41] H. Sieurin, R. Sandström, Sigma phase precipitation in duplex stainless steel 2205, Mater. Sci. Eng., A 444 (2007) 271–276.
[42] E. Rabinowicz, L.A. Dunn, P.G. Russell, A study of abrasive wear under three-body conditions, Wear 4 (1961) 345–355.
[43] J.F. Tavernekku, L.F. Coffin., A compilation and interpretation of cyclic/strain fatigue tests, Trans. ASM 51 (1959) 438–450.
[44] ASM Handbook, Volume 1, Properties and Selection: Irons, Steels, and High Performance Alloys, ASM International, Materials Park, OH, 2005.
[45] M.A.L. Hernández-Rodríguez, R.D. Mercado-Solís, A.J. Pérez-Unzueta, D.I. Martinez-Delgado, M. Cantú-Sifuentes, Wear of Cast Metal–Metal Pairs for Total Replacement Hip Prostheses, 259 (2005) 958–963.
[46] Y.P. Li, Y. Yamashita, N. Tang, B. Liu, S. Kurosu, H. Matsumoto, Y. Koizumi, A. Chiba, Influence of carbon and nitrogen addition on microstructure and hot deformation behavior of biomedical Co–Cr–Mo alloy, Mater. Chem. Phys. 133 (2012) 849–854.
[47] A.J. Saldívar-García, H.F. López, Microstructural effects on the wear resistance of wrought and as-cast Co–Cr–Mo–C implant alloys, J. Biomed. Mater. Res. Part A 74A (2005) 269–274.

[48] K. Rajan, Phase transformation in a wrought Co–Cr–Mo–C alloy, Metall. Trans. A 13 (1982) 1161–1166.
[49] A. Salinas-Rodriguez, J.L. Rodriguez, Deformation behavior of low-carbon Co–Cr–Mo alloys for low-friction implant applications, J. Biomed. Mater. Res. 31 (1996) 409–419.
[50] C. Montero-Ocampo, M. Talavera, H. Lopez, Effect of alloy preheating on the mechanical properties of as-cast Co–Cr–Mo–C alloys, Metall. Mater. Trans. A 30 (1999) 611–620.
[51] S.H. Lee, E. Takahashi, A. Nomura, Chiba, Effect of carbon addition on microstructure and mechanical properties of a wrought Co–Cr–Mo implant alloy, Mater. Trans. 47 (2006) 287–290.